npj | climate and atmospheric science

Article

Published in partnership with CECCR at King Abdulaziz University

https://doi.org/10.1038/s41612-024-00889-7

Cloud microphysical response to entrainment of dry air containing aerosols

Jae Min Yeom[1] ✉, Hamed Fahandezh Sadi[1], Jesse C. Anderson[1], Fan Yang[2], Will Cantrell[1] ✉ & Raymond A. Shaw[1] ✉

Impacts of aerosol particles on clouds, precipitation, and climate remain one of the significant uncertainties in climate change. Aerosol particles entrained at cloud top and edge can affect cloud microphysical and macrophysical properties, but the process is still poorly understood. Here we investigate the cloud microphysical responses to the entrainment of aerosol-laden air in the Pi convection-cloud chamber. Results show that cloud droplet number concentration increases and mean radius of droplets decreases, which leads to narrower droplet size distribution and smaller relative dispersion. These behaviors are generally consistent with the scenario expected from the first aerosol-cloud indirect effect for a constant liquid water content (L). However, L increases significantly in these experiments. Such enhancement of L can be understood as suppression of droplet sedimentation removal due to small droplets. Further, an increase in aerosol concentration from entrainment reduces the effective radius and ultimately increases cloud optical thickness and cloud albedo, making the clouds brighter. These findings are of relevance to the entrainment interface at stratocumulus cloud top, where modeling studies have suggested sedimentation plays a strong role in regulating L. Therefore, the results provide insights into the impacts of entrainment of aerosol-laden air on cloud, precipitation, and climate.

Aerosol-cloud interactions have been intensively debated in the past few decades, but still remain one of the large uncertainties in global climate models[1,2]. Evidence indicates that aerosols can modify the microphysical properties of clouds (e.g., cloud droplet number concentration (N_c), liquid water content (L), mean radius of droplets (r_m), etc.), resulting in a further impact on cloud cover, precipitation, and lifetime of clouds[3–7]. Increasing aerosol number concentration is generally considered to offset climate warming because it leads to an increase of N_c and a decrease of r_m, thereby increasing reflection of sunlight back to space and slowing precipitation droplet formation. However, the sign and magnitude of aerosol-induced change in cloud microphysics are highly uncertain due to the complex nonlinear interactions between aerosol and cloud under various thermodynamic and dynamical conditions[8,9]. Global climate models have difficulties capturing such cloud and aerosol processes because they rely on parameterizations of these processes that can be empirical and incomplete, which causes large variations in the climate change predictions.

Stratocumulus clouds are of particular interest because of their role in determining Earth's climate. One of the primary controlling factors for stratocumulus cloud properties is the entrainment of warm, dry air that occurs at cloud top[10]. The entrainment interfacial layer (EIL) where this mixing occurs is small in vertical extent compared to typical cloud and boundary layer thicknesses, and is highly variable and intermittent[11–13]. Entrainment also influences strongly on cloud microphysical properties for cumulus clouds and even deep convection and it remains a key challenge to represent in coarse resolution models[14,15]. Entrainment-mixing influences cloud microphysical properties differently depending on how the mixing between cloudy and clear air proceeds[16–21]. Reduction in cloud liquid water content $L \propto N_c d^3$ can occur through uniform reduction of the diameter of all droplets, or in the other limit, can occur through the complete evaporation of a subset of droplets leaving the remaining ones unchanged. These limits are referred to as homogeneous and inhomogeneous mixing, respectively.

Not only does entrainment influence cloud properties, but details of cloud microphysical processes turn out to be highly important in determining the strength of entrainment at stratocumulus cloud top. These feedbacks strongly influence the way such clouds respond to changes in the cloud droplet concentration and size through aerosol perturbations. Two entrainment effects have been identified. The sedimentation-entrainment effect results from smaller droplets having weaker sedimentation, and therefore maintaining higher liquid water content within the cloud-top entrainment region[5,7,22]. The evaporation-entrainment feedback results

[1]Department of Physics and Atmospheric Sciences Program, Michigan Technological University, Houghton, USA. [2]Brookhaven National Laboratory, Upton, USA. ✉e-mail: jyeom2@mtu.edu; cantrell@mtu.edu; rashaw@mtu.edu

from smaller droplets allowing for more efficient evaporation during cloud-top entrainment[23]. As pointed out by Hoffmann et al.[24], it depends on the phase relaxation time, which in turn depends inversely on the number concentration and mean radius of cloud droplets, resulting in time scales of the order of 1−10 s. It is therefore challenging to resolve in a typical large eddy simulation. Local (sub-grid scale) sedimentation effects are also unable to be resolved. Consequently, experiments that fully resolve the evaporation and sedimentation processes, such as those presented here, are of value for understanding evaporation and sedimentation interactions during mixing, even though the feedbacks to the entrainment rate itself are not included.

Numerous observational studies have focused on what type of mixing mechanism occurs dominantly under the assumption that the impact of entrained aerosols on clouds is negligible. However, in aerosol-laden environments, entrained aerosols might be a pivotal factor in entrainment processes due to their ability to act as cloud condensation nuclei (CCN) (e.g., secondary activation of droplets), thereby influencing cloud microphysical and radiative properties. Previous studies have suggested that the secondary activation of droplets above cloud base could affect significantly not only the cloud microphysical and radiative properties but also cloud lifetime and precipitation efficiency[25–28]. The entrained aerosols could contribute a significant portion of total activation, which becomes more important as aerosol concentration increases. Secondary activation of droplets also can slow down the cloud droplet radius growth rate, thereby making clouds brighter[29,30]. The recent work[31] shows that increasing aerosol concentration above an Arctic low-level cloud results in a precipitation suppression due to less efficient collision-coalescence process from an increase in cloud droplet number concentration and a decrease in droplet size. As a result, the clouds have a high liquid water content in high aerosol concentration simulations, which enhances cooling at cloud top and drives strong vertical motions in the clouds. The importance of the role of entrained aerosols is obvious for a better understanding of cloud-aerosol interactions, but it is still difficult to find direct evidence for the effects of secondary activation process across scales in the observational studies due to the limitations of measurements.

Recently, we investigated the cloud microphysical responses to different entrainment conditions based on experiments conducted in the Pi convection-cloud chamber[21]. In those experiments, the entrained air did not contain aerosol particles. When aerosol particles are entrained at the stratocumulus cloud top, several key physical processes occur, significantly influencing the formation, structure, lifetime, and radiative properties of the cloud[32]. For example, some of the entrained aerosols serve as CCN, which not only alters cloud droplet size distribution but also affects cloud lifetime and precipitation efficiency. Quantifying the effects of entrained aerosol requires a combination of observations and modeling studies to understand the complex mechanisms of aerosol-cloud interactions.

To focus on the impacts of entrained aerosols on cloud properties within the EIL at the stratocumulus cloud top, we have conducted experiments in which aerosol particles are added to the entrained air. All controllable parameters, such as temperature, flow rate, and relative humidity of entrained air, are fixed at the same values for all experiments, but the sizes of aerosol particles in the entrainment flow differ for each experiment. This experimental design will not capture radiative cooling processes and related feedbacks, but the results provide insight into the effects of entrained aerosols on clouds, while avoiding complicating feedback from other factors.

We begin by explaining the experiment setup in more detail and then show the observational results, emphasizing the variations in cloud droplet size distribution and then interpret adjustments of L in light of simple models for the convection-cloud chamber. We describe a decrease in the relative dispersion of droplet size distributions due to entrained aerosols and also present integrated quantities such as cloud liquid water content and cloud radiative properties for each experiment. Finally, we discuss the atmospheric implications of these idealized laboratory results, specifically for aerosol and sedimentation effects on cloud liquid water content.

Results

Overview of experiment

Experiments for investigating the impacts of aerosols in entrained air on clouds are conducted in the Pi chamber. This laboratory facility is able to create a cloud through a temperature difference between water saturated top and bottom plates (moist Rayleigh-Bénard convection). When the source of cloud droplets from aerosol injected into the chamber is balanced by subsequent sedimentation of cloud droplets, the steady-state in an individual experiment is achieved and then sustained for hours (see the details of the chamber in Chang et al.[33]).

Yeom et al. (2023)[21] conducted entrainment experiments by injecting dry and particle-free air through a temperature-controlled flange in the top boundary. This study showed that cloud microphysical responses to entrainment and mixing are different on microphysical and systemwide scales. However, the impacts of the secondary droplet activation due to the entrained air were not considered because the entrained air did not contain aerosol particles.

How are the cloud responses different if aerosol particles are in the entrained air? To answer this question, we add aerosols of different sizes in entrained air as shown schematically in Fig. 1. The temperatures of the top, sidewall, and bottom surfaces of the main portion of the chamber are set to 12 °C, 20 °C, and 28 °C, resulting in an unstable temperature difference of $\Delta T = 16$ °C and a mean temperature of 20 °C. The moist Rayleigh-Bénard convection conditions are held for a few hours, and then NaCl particles, size selected at 130 nm, are injected at a constant rate to achieve the steady-state cloud condition (called "Background"). Once steady-state cloud conditions have been achieved, air is injected into the cloudy region through the entrainment zone. The temperature, relative humidity, and flow rate of entrained air are fixed at 30 °C, 20%, and 20 liters per minute (LPM), respectively, for all entrainment experiments. However, the sizes of NaCl particles (50, 130, and 300 nm) contained in entrained air are different for different experiments. The cloud reaches another steady state, different than the background condition for a given entrainment condition (i.e., the size of aerosol particles in entrained air). The important thing to note is that the injection rate of entrained aerosols is the same as that of the background cloudy condition. This is not typical, but it is occasionally observed in marine stratocumulus clouds[34]. We measure cloud droplet size distributions at one fixed measurement position after each steady-state cloudy condition is achieved under different entrainment conditions.

One of the key advantages of these experiments under controlled conditions is that we can explore directly how the cloud microphysical properties change due to the secondary droplet activation. In this respect, the experiments presented here can provide valuable implications for understanding the impacts of aerosols on clouds, precipitation, and climate.

Effect of Aerosols in Entrained Air on Droplet Size Distributions

Figure 2 shows the non-normalized and normalized mean droplet size distributions for each steady-state condition. All droplet size distributions show a bimodal shape with two peaks. These peaks are related to haze and cloud droplets, respectively. Compared to the background condition that represents the steady state cloudy condition without entrainment, the droplet size distribution of aerosol-free condition (with the entrainment, but not containing aerosol particles) is slightly shifted to smaller sizes because the entrained dry air not including aerosol particles just evaporates the droplets. Such behavior is consistent with a homogeneous mixing response. However, due to high temperature gradient (16 K), the magnitude of a shift to smaller sizes is smaller than 10 K experiments in Yeom et al.[21], even though the relative humidity of entrained air is lower in these experiments. The mean supersaturation from a scalar flux-budget analysis[21] is about 5.5% in the cloud-free condition. Such high supersaturation is a result of strong boundary fluxes relative to entrainment flux, which supports the small shift to smaller sizes.

The changes in droplet size distributions from the background condition are dramatically different when the entrained air contains aerosol particles. The number concentrations of haze and cloud

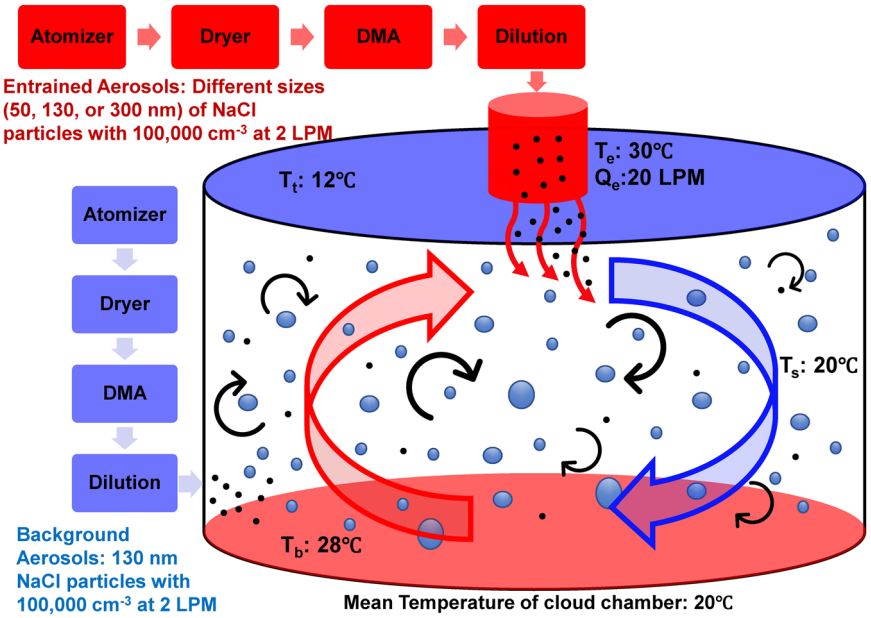

Fig. 1 | An overview of the experiment. The temperatures of the top, sidewall, and bottom surfaces are set to 12 °C, 20 °C, 28 °C, respectively. The temperature and flow rate of entrained air are 30 °C and 20 liters per minute (LPM) for all experiments. For the background cloudy condition, NaCl particles, size selected at 130 nm by the Differential Mobility Analyzer (DMA), are injected at a constant rate (100,000 cm^{-3} at 2 LPM). Additionally, different sizes of NaCl particles (50, 130, 300 nm) selected by the DMA are injected through entrainment zone at the same rate. The black and blue circles represent aerosol particles and droplets, respectively. The direction of large scale circulation in the chamber is shown with red and blue curved arrows.

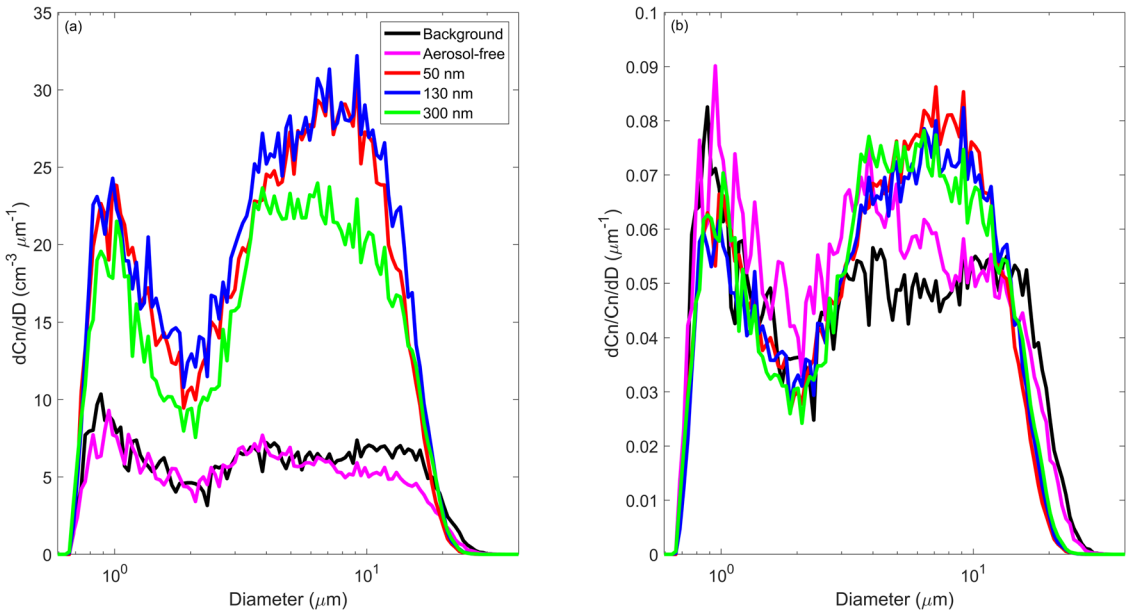

Fig. 2 | Mean droplet size distributions under each steady state cloudy condition. **a** Nonnormalized and **b** normalized mean droplet size distributions under each steady state cloudy condition. Background represents the steady state cloudy condition without entrainment; Aerosol-free represents the steady state cloud under 30 °C and 20 LPM entrained air condition without aerosols; 50 nm, 130 nm, and 300 nm indicate the steady state clouds under 30 °C and 20 LPM entrained air condition with the different sizes of aerosols (50 nm, 130 nm, and 300 nm).

droplets (N_h and N_c) increase significantly because the aerosol concentration inside the chamber increases by approximately a factor of two. The shapes of these droplet size distributions are shifted to smaller sizes than in the aerosol-free entrainment condition—specifically, note the right tail of the distributions. The normalized droplet size distributions for the 50, 130, and 300 nm cases are almost identical in shape, but the overall number concentration is lower for the 300 nm case compared to the other two cases. We do not have a rigorous explanation for this behavior, but we expect that it may be a result of kinetically-limited activation and growth of large 300-nm salt aerosols[35]. Ongoing experiments and comparisons with a detailed microphysics model should shed more light on this interesting possibility.

Response of Liquid Water Content *L*: Theory Versus Observed

Our common understanding is that L inevitably decreases when entrainment of warm and dry air occurs[17–19,21,36]. Consistent with that expectation, L decreases in the aerosol-free entrainment case due to the evaporation of droplets. However, L increases significantly when the entrained air contains aerosol particles. Such behavior apparently contradicts the expected reduction of L due to entrainment. The behavior is illustrated in Fig. 3 by the data points corresponding to the background and four different entrainment cases. Consistent with the size distributions in Fig. 2a, the droplet concentration is higher in the cases with entrained air containing aerosol particles. And the liquid water content is as much as 50% greater in the aerosol-laden entrainment cases compared to the background, and about a factor of 2 larger than the case with aerosol-free entrainment. This behavior can be

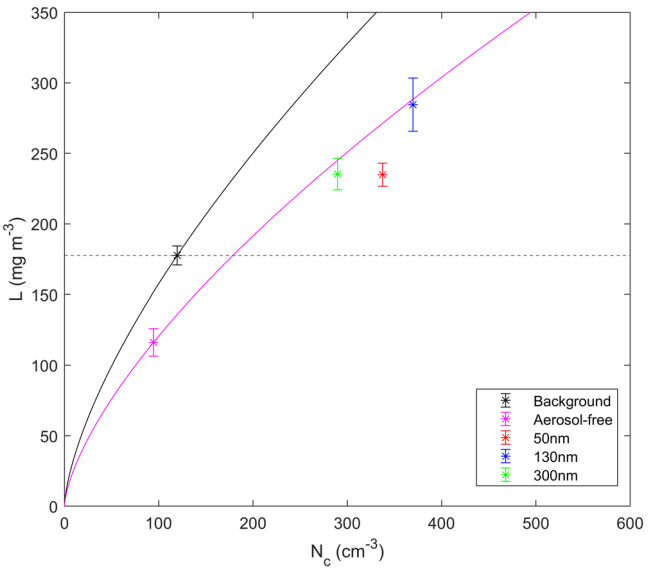

Fig. 3 | Cloud droplet number concentration (N_c) versus liquid water content (L) for all experiments. Mean and standard error of N_c and L are denoted for each condition. Each line is a best-fit power law with exponent of 2/3 based on mean values of N_c and L of Background and Aerosol-free conditions, respectively. The dashed line represents the mean value of L under the Background condition, which serves as a reference to distinguish two regimes based on the aerosol number concentration in the entrained air.

understood qualitatively as suppressed droplet sedimentation removal resulting from the smaller cloud droplet diameters when aerosols are added with the entrained air (cf. Fig. 2b). We provide an overview of a quantitative comparison here, and return to a more detailed treatment in the discussion.

A theoretical model of the microphysical properties in a convection-cloud chamber can be developed by considering mass and number balances for cloud droplets[37,38]. For the "fast microphysics" regime that is relevant under relatively high-aerosol conditions, the model predicts L is proportional to the number concentration of injected aerosols ($N_{inj}^{2/3}$)[38]. This assumes that all injected aerosols become cloud droplets, but of course it is more complicated for more polluted clouds in the real chamber experiments because some portion of aerosol particles is not activated to form cloud droplets and remain as haze droplets. As an approximation, we can use N_c instead of N_{inj} for the liquid water scaling, as has been shown to be consistent with Pi Chamber measurements[38]. The result allows us to understand why L increases significantly when entrained air contains aerosol particles, as illustrated by the curves in Fig. 3, which represent power laws with exponent 2/3, passing through from the data points for the background conditions (black) and for aerosol-free-entrainment conditions (magenta). L of the aerosol-free condition decreases from the background condition because droplets are evaporated due to dry air entrainment and then the cloud reaches the new steady-state with lower L. It is intriguing to note that the three data points for entrainment with aerosol (50, 130, and 300 nm) reside reasonably close to the 2/3 scaling law extended from the data point for aerosol-free entrainment. The L values of those three cases are all significantly smaller than the predicted L scaling from the background condition, but they are larger than the background condition itself.

The agreement with the fast-microphysics scaling implies the following. First, the effect of evaporation reduces points to a common $N_c - L$ contour in Fig. 3 because the entrained dry air properties are the same for all experiments. Second, due to the addition of aerosol particles from entrained air, liquid water is apportioned differently. In essence, the competition between cloud droplets becomes more intense when the aerosol concentration is increased, resulting in a decrease of mean droplet size. Smaller cloud droplets have longer residence times because the efficiency of sedimentation decreases. Under steady-state conditions, the observed L is strongly influenced by the droplet residence time and as a result, the clouds influenced by entrained aerosol retain more liquid water. According to the theoretical estimation, the change in L due to entrained aerosols would be different depending on the aerosol properties (e.g., number concentration). In Fig. 3, both N_c and L gradually increase from the aerosol-free condition as the aerosol number concentration in the entrained air increases. This behavior can be understood by considering two regimes, using the mean liquid water content of the background condition as a reference. When the aerosol concentration in the entrained air is low, the liquid water content remains lower than the background value because the evaporation effect from dry air entrainment is still more important than the sedimentation effect. In contrast, when the aerosol concentration in the entrained air increases, the liquid water content becomes larger than the background value, indicating that the sedimentation effect has become the dominant factor. Exploring the response of L depending on the aerosol properties in the entrained air will be the focus of future work.

Relationship Between Relative dispersion and Cloud Droplet Number Concentration

The changes in the spectral shape of the size distribution of cloud droplets due to the aerosol particles in entrained air are evident as shown in Fig. 2. Variation in the spectral dispersion of cloud droplet size distribution can be represented by the relative dispersion

$$\epsilon = \frac{\sigma_r}{r_m}, \tag{1}$$

where r_m is the mean radius of cloud droplets and σ_r is the standard deviation of cloud droplet size distribution. ϵ is of relevance to the indirect aerosol effect (Twomey effect) and influences the calculation of the effective radius (r_e) frequently used in climate models[39–42]. However, there is no clear agreement regarding whether the the cooling effect as predicted by the Twomey effect is enhanced or suppressed depending on the variation of ϵ with increased aerosol loading. To better understand how the dispersion effect modifies the Twomey effect, the dispersion offset (DO) is defined as the ratio of dispersion effect to aerosol indirect effect:

$$DO = -\frac{3dln\beta}{dlnN_c}, \tag{2}$$

where β is the effective radius ratio and is positively dependent on ϵ, assuming a gamma distribution[39,43,44]. If the correlation between ϵ and N_c is negative under similar L conditions, the dispersion offset is positive, indicating that the dispersion effect enhances the cooling.

Here we consider the dispersion effect resulting from dry air entrainment with aerosol particles. Figure 4 shows the relationships between r_m and σ_r, and N_c and ϵ for all experiments. Compared to the background condition, r_m and σ_r slightly decrease in the aerosol-free case due to the evaporation of cloud droplets. However, all values of ϵ for the aerosol-free condition increase because r_m decreases more than σ_r. When the entrained air contains aerosol particles, both r_m and σ_r decrease simultaneously. The values of ϵ also decrease with the increase of N_c because the reduction of σ_r is larger than r_m. Such behavior is consistent with the positive dispersion offset scenario for enhancing the cooling of the Twomey effect. The entrained dry air evaporates the cloud droplets and entrained aerosol particles make the competition between droplets for water vapor more intense relative to the aerosol-free condition. Therefore, the entrainment containing aerosol particles causes not only a decrease in mean droplet size but also a narrowing of the cloud droplet size distributions, which can make the droplet residence time longer and the droplet settling speed slower, respectively. As a consequence of these effects, the important thing to note is that the dispersion effect due to the high number concentration of low dispersed cloud droplets can enhance the cooling effect on the climate.

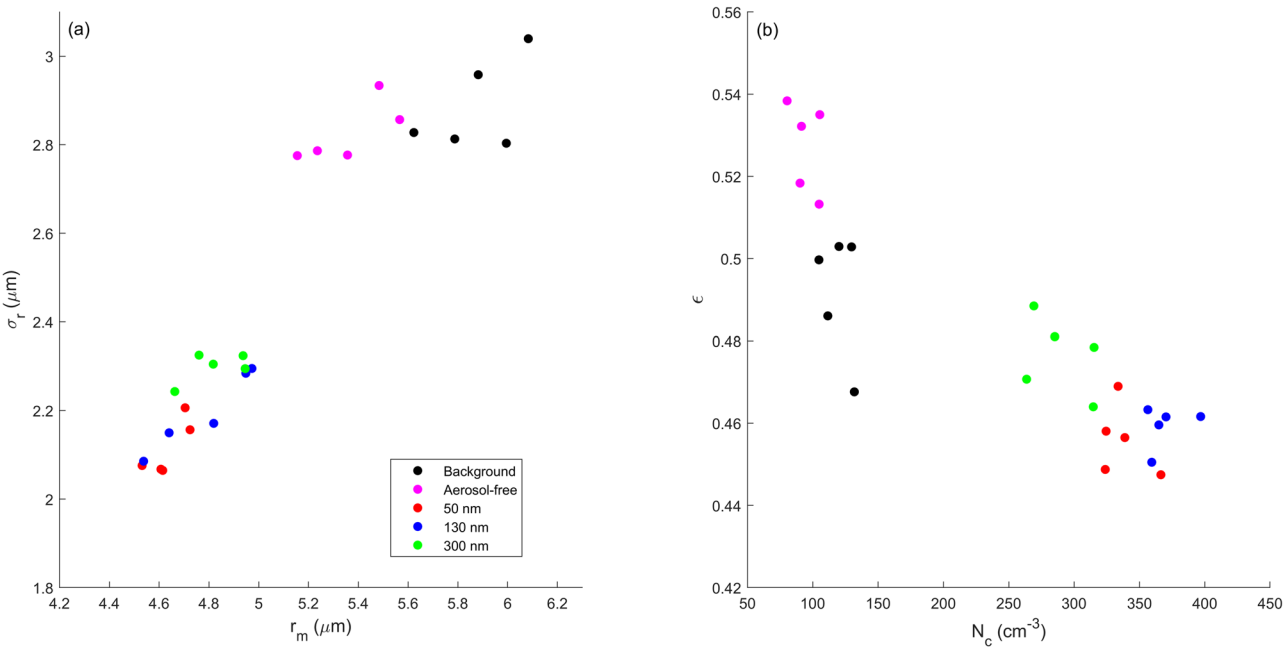

Fig. 4 | Variation in the spectral dispersion of cloud droplet size distribution. a Relationships between mean radius of cloud droplets (r_m) and standard deviation of radius (σ_r) for all experiments. **b** The relationships between cloud droplet number concentration (N_c) and relative dispersion (ϵ) for all experiments.

Implication for Cloud Brightening

The cloud radiative properties such as r_e, cloud optical thickness (τ), and albedo (A_c) are changed significantly via the modification of cloud microphysical variables (e.g., number concentration, size, and spectral shape of distribution). Figure 5 shows that the clouds reach a new steady state with higher N_c, N_h, and L as dry air including aerosol particles is entrained into the chamber. We now explore how the radiative properties of these cloud are changed by entrained aerosol particles, which provides insight into aerosol indirect effects.

Microphysical properties in the Pi Chamber are closely representative of those that would exist in a stratocumulus cloud[42,45]. The radiative properties of a cloud, including optical thickness τ and albedo A_c depend on the effective radius r_e, as mentioned above. This can be calculated as the ratio between the third and second moment of the cloud droplet size distribution. By using this, τ and A_C are calculated as[29,46]

$$\tau = \frac{3}{2\rho_w}\int_0^h \frac{\rho q_l}{r_e}dz \tag{3}$$

and

$$A_c = \frac{\tau}{\gamma + \tau} \tag{4}$$

where ρ_w is water density; ρ is air density; q_l is liquid water mixing ratio; γ is assumed to be 13.3, which depends on the degree of forward scattering for overhead sun[47]. The q_l inside the clouds is not uniform. However, we assume that q_l is constant from 0 to 10 m for comparison, as the thickness of the entrainment interfacial layer is typically on the order of several tens of meters.

As shown in Fig. 5d, all values of r_e in the aerosol-free, 50, 130, 300 nm cases decrease from the background condition, but the enhancement of aerosols increases N_c, resulting in a much stronger decrease of r_e in those cases. As a result, τ and A_c increase significantly for the 50, 130, 300 nm cases (Fig. 5e, f). Interestingly, the case of 130 nm shows the highest values of N_c, L, τ, and A_c. The comparison between 50, 130, and 300 nm cases might imply an additional role of entrained aerosol size, in addition to concentration, for determining cloud optical properties[29,48]. In the cases with 50 nm and 300 nm aerosols entrained into a background cloud containing aerosols of 130 nm, the difference in efficiency of activation of small versus large aerosol particles may lead to somewhat lower cloud droplet concentrations compared to the case when both background and entrained aerosols are 130 nm. This apparently is secondary to the most significant influence on droplet size and liquid water content that are driven primarily by the increase in total aerosol injection rate. There are slight differences between three cases, but the effects of aerosol particles in entrained air are prominent and imply that the enhancement in N_c due to entrained aerosols can make clouds brighter and more reflective. The nonlinear scaling of L is important to this conclusion, and its relevance to atmospheric clouds will be discussed in the next section.

Discussion

The experimental results reported here provide evidence for the impacts of entrained aerosol particles on cloud top microphysical properties. The addition of aerosols through entrained air increases N_c and decreases r_m, which leads to narrower cloud droplet size distributions and brighter clouds. This result is generally consistent with the scenario expected from the first aerosol-cloud indirect effect (Twomey effect) for a constant L. However, in these experiments, L increases significantly as shown in Fig. 3. This response to entrainment is surprising, and as mentioned already, such behavior can be understood as suppression of droplet sedimentation removal due to the smaller cloud droplet diameters when aerosols are added with the entrained air. When is this type of sedimentation effect of relevance in natural clouds?

Over the last few decades there has been a growing recognition of the role droplet sedimentation plays in the response of clouds to entrainment. Considine and Curry[49] recognized that the strong segregation of clear and cloudy air inherent to a high-Peclet-number system like cloud droplets in air, typically referred to as inhomogeneous mixing, can be overcome through droplet sedimentation. Specifically, sedimentation transports cloud droplets from cloudy regions to clear-air regions during the mixing process. Later, using large eddy simulation, it was recognized that sedimentation can also play a significant role in removing liquid water from the entrainment interfacial layer (EIL) at the top of stratocumulus clouds, thereby influencing the evaporative cooling at cloud top[5,7,22]. Such sedimentation effects can have a similar magnitude of influence on entrainment strength as processes directly involved in turbulence production, like velocity

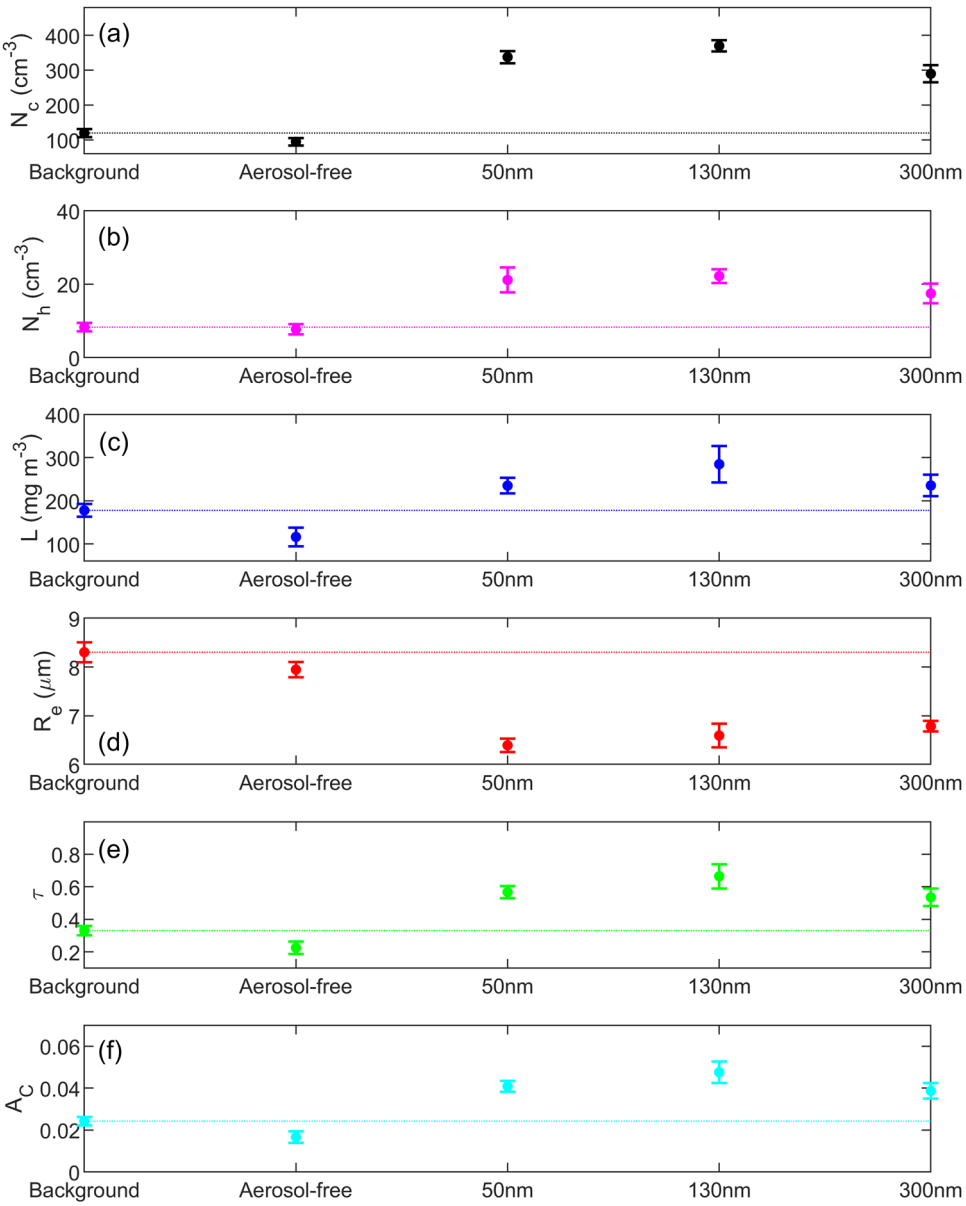

Fig. 5 | Cloud microphysical and radiative properties for each experiment. Mean and standard error of **a** cloud droplet number concentration (N_c), **b** haze droplet number concentration (N_h), **c** liquid water content (L), **d** effective radius (R_e), **e** cloud optical thickness (τ), **f** cloud albedo (A_c) for each experiment. The horizontal dashed lines indicate the mean value of Background condition.

shear[50]. To draw a connection to this work, the idealized cloud chamber experiments presented here can be envisioned as representing the cloud-top, EIL where sedimentation of cloud droplets directly influences the amount of liquid water. To make more rigorous connections, we consider the details of how sedimentation and liquid water are connected in a convection-cloud chamber.

Idealized models of the microphysical properties existing in a convection-cloud chamber show that the liquid water content is largely determined by the supersaturation forcing, and by the droplet removal rate through sedimentation[37,38]. The sedimentation rate, in turn, depends on the square of the droplet diameter (assuming Stokes drag), and as a result, higher aerosol concentrations that lead to smaller cloud droplet diameters result in clouds with higher liquid water content. This is consistent with observed behavior in the cloud chamber[37,51]. Following Shaw et al.[38], a solution for liquid water content can be obtained for the fast microphysics limit, in which the cloud droplet phase relaxation time is much less than the time scale for replenishment of the supersaturation field. This limit is generally valid for stratocumulus clouds[45]. A mass budget for the convection-cloud chamber requires that the condensation rate is equal to the precipitation rate. Assuming the time scale for removal of mass is equal to L/τ_{res}, where $\tau_{res} = H/v_T$, $v_T = kr^2$ is the Stokes terminal fall speed, and H is the chamber height. Therefore

$$n\rho_l \frac{4}{3}\pi r^3 \frac{v_T(r)}{H} = n\rho_l 4\pi r \xi s, \tag{5}$$

and in steady state the supersaturation is

$$s = s_0\left(1 + \frac{\tau_t}{\tau_c}\right)^{-1}, \tag{6}$$

where τ_t is a turbulent mixing time and $\tau_c = (4\pi D' nr)^{-1}$ is the phase relaxation time, with D' being a modified diffusion coefficient[51]. In the fast microphysics limit, typically valid even for moderate cloud droplet concentrations, this can be approximated as $s \approx s_0\tau_c/\tau_t$, which implies

$$s \propto \frac{\dot{s}}{nr}, \tag{7}$$

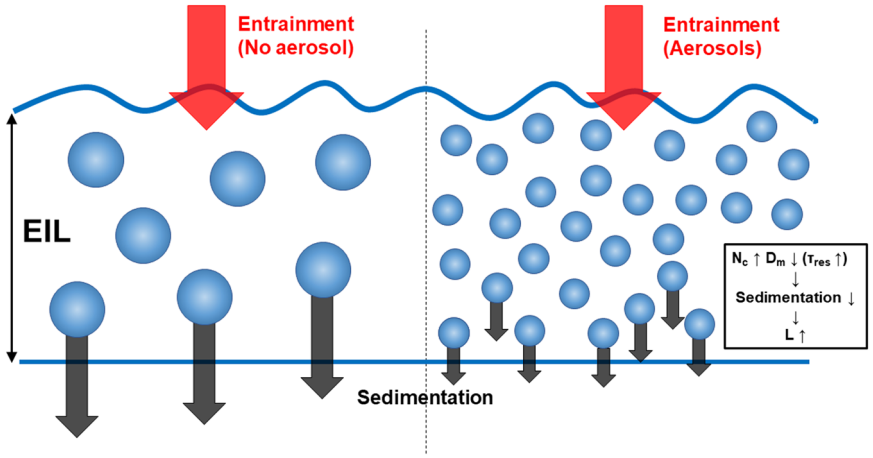

Fig. 6 | A schematic illustration of the droplet sedimentation removal within the entrainment interfacial layer (EIL) under different entrainment conditions. The mean size of cloud droplets and their settling speeds are shown schematically for entrainment of dry air that contains aerosols (right) or does not (left). The addition of aerosols in entrained air leads to increased cloud droplet number concentration (N_c), decreased mean diameter of droplets (D_m), and increased residence time scale (τ_{res}). As a result, the droplet sedimentation is suppressed and liquid water content (L) increases within the EIL when the entrainment flow contains aerosols.

where we have defined $\dot{s} = s_0/\tau_t$ as a rate at which supersaturation is replenished through turbulent mixing. Note that this is exactly analogous to the expression for quasi-steady supersaturation in a parcel rising at speed w, for which $s \propto w/(n r)$. Plugging Equation (7) into Equation (5) and simplifying leads to a conveniently compact expression for liquid water content:

$$L = \frac{\rho_l \xi}{D'} \tau_{res} \dot{s}. \tag{8}$$

Its proportionality with $\tau_{res} = H/v_T(r)$ has the important implication that liquid water content scales with droplet radius as $L \sim r^{-2}$. This result can be further simplified by considering a number budget with the injection rate of aerosols $\dot{n}_{in}$ equated to the cloud droplet residence time due to sedimentation. Then droplet radius can be eliminated and a scaling law $L \propto \dot{n}_{in}^{2/3}$ is obtained[38]. This is the expression underlying the curves in Fig. 5.

Extending this argument to the EIL at the top of a stratocumulus cloud is possible because of similar fundamental processes existing in a convection-cloud chamber. As shown schematically in Fig. 6, sedimentation is one of the most important sink mechanisms of L within the EIL. The sedimentation flux out of the EIL strongly depends on cloud droplet size. The addition of aerosols through entrainment could tend to increase cloud droplet number concentration and decrease the mean diameter of droplets. As a result, the removal of droplets through sedimentation is suppressed, which leads to an increase of L within the EIL. This is consistent with previous simulation results that L in the entrainment zone can be enhanced if neglecting droplet sedimentation in the model[7].

In this hypothetical scenario, L within the EIL could continuously increase due to the suppression of droplet sedimentation. However, this increase of L within the EIL in natural clouds may enhance the evaporative cooling of mixtures of cloudy and entrained air and cloud-top radiative cooling because of the high number concentration of small droplets, making it easier for the entrained air to sink[5,7,22]. Consequently, entrainment develops through the enhancement of turbulence associated with buoyancy reversal. However, such feedback does not exist in the Pi Chamber because the entrainment rate is fixed during the experiments.

The net impact of entrained aerosol-laden dry air on L within the EIL depends on the competition of radiation cooling, feeding of undiluted cloud from below, entrainment-induced evaporation, and droplet sedimentation. We may speculate based on our experimental findings, therefore, that the presence of aerosols in the free troposphere will have a tendency to break up the stratocumulus clouds by strengthening the evaporation-entrainment feedback. Searching for evidence of this in stratocumulus observations or LES would be of interest.

We conclude by acknowledging that the sign and magnitude of aerosol-induced effects on clouds are sensitive to environmental conditions as well as energy/water budget constraints[31,52–56]. Substantial effort has been made to improve the understanding of aerosol-induced effects depending on environmental regimes. However, the variability in the real atmospheric cloud conditions causes large uncertainty regarding the relative importance among multiple aerosol effects across the spatial and temporal scales. The results reported here are from one specific cloud scenario, in which dry air containing aerosols is entrained into a cloud, and further suggest the need for research on how entrained aerosol properties (e.g., aerosol number concentration) affect cloud microphysical properties. Especially in the context of the EIL at stratocumulus cloud top, in which cloud droplet sedimentation from the top layer is known to play an important role, this aerosol entrainment effect has the potential to strongly influence not only the microphysical properties of the cloud, but the overall cloud dynamics through evaporative and radiative cooling. This set of idealized laboratory results can therefore shed light on the understanding of cloud-aerosol interactions, especially with regard to the cloud responses to entrainment of dry air containing aerosols.

Methods

Experiment set-up and data

As described in Fig. 1 in the main text, the moist Rayleigh-Bénard convection conditions with $\Delta T = 16$ °C were held for a few hours to ensure stable temperatures across all surfaces and then NaCl particles, size selected at 130 nm using a Differential Mobility Analyzer (DMA), were injected at a constant rate (100,000 cm^{-3} at 2 LPM) for the background condition. Once a steady-state cloud condition of the background were achieved, we first measured background cloud droplet size distributions with a Welas-2000 optical particle counter covering a diameter range of 0.583 to 40.679 μm, prior to the entrainment events. The size of NaCl particles in entrained air was also selected at 50, 130, or 300 nm by a DMA for different entrainment experiments. The injection rate of NaCl particles through the entrainment flange was almost the same as the background condition. The temperature, humidity, and flow rate of entrained air were fixed at 30 °C, 20%, and 20 LPM, respectively. This flow rate corresponds to an entrainment velocity of 1.5 cm s^{-1}, which is comparable to that in the real atmosphere[57]. For the measurements of cloud droplet size distributions as well as interstitial and residual particles, we sampled the air at a flow rate of 7 liters per minute. The excess air was diverted through another tube. Five samples are obtained for each steady-state condition achieved by different entrainment conditions, and each sample was measured for 100 s.

Haze and cloud droplets

The critical diameter of the aerosol (d_c) is generally used to divide into haze ($d < d_c$) and cloud ($d > d_c$) droplets from the size distribution of the droplets. We used 130 nm NaCl particles for the background cloud condition and three different sizes (50, 130, and 300 nm) of NaCl particles in the entrained air. The critical diameters of these NaCl particles are roughly 1, 2, and 6 μm, respectively. In an environment condition where aerosols of two different

sizes are mixed, it is difficult to distinguish between haze and cloud droplets based on size alone because the size ranges of haze and cloud droplets can overlap. Figure S1 shows the cloud (N_c) and haze (N_h) droplet number concentrations depending on different values of d_c for all experiments. As the critical diameter increases, N_c decreases, and N_h increases. The trend is the same for all experiments because the the number concentration with different critical diameters is just scaled down and up. Therefore, we decided to use $d_c = 2\mu m$, the critical diameter of the 130 nm NaCl particles used in the background condition, as a threshold to distinguish between haze and cloud droplets.

Data Availability

Data required to reproduce figures have been deposited in Digital Commons (https://doi.org/10.37099/mtu.dc.all-datasets/56).

Received: 17 October 2024; Accepted: 21 December 2024;
Published online: 08 January 2025

References

1. Stevens, B. & Feingold, G. Untangling aerosol effects on clouds and precipitation in a buffered system. *Nature* **461**, 607–613 (2009).
2. Stier, P. et al. Multifaceted aerosol effects on precipitation. *Nat. Geosci.* **17**, 719–732 (2024).
3. Twomey, S. Pollution and the planetary albedo. *Atmos. Environ.* **8**, 1251–1256 (1974).
4. Albrecht, B. A. Aerosols, cloud microphysics, and fractional cloudiness. *Science* **245**, 1227–1230 (1989).
5. Ackerman, A. S., Kirkpatrick, M. P., Stevens, D. E. & Toon, O. B. The impact of humidity above stratiform clouds on indirect aerosol climate forcing. *Nature* **432**, 1014–1017 (2004).
6. Xue, H. & Feingold, G. Large-eddy simulations of trade wind cumuli: Investigation of aerosol indirect effects. *J. Atmos. Sci.* **63**, 1605–1622 (2006).
7. Bretherton, C., Blossey, P. N. & Uchida, J. Cloud droplet sedimentation, entrainment efficiency, and subtropical stratocumulus albedo. *Geophysical Research Letters* **34**, https://doi.org/10.1029/2006GL027648 (2007).
8. Gryspeerdt, E. & Stier, P. Regime-based analysis of aerosol-cloud interactions. *Geophys. Res. Lett.* **39** (2012).
9. McCoy, D. T. et al. Aerosol midlatitude cyclone indirect effects in observations and high-resolution simulations. *Atmos. Chem. Phys.* **18**, 5821–5846 (2018).
10. Mellado, J. P. Cloud-top entrainment in stratocumulus clouds. *Annu. Rev. Fluid Mech.* **49**, 145–169 (2017).
11. Katzwinkel, J., Siebert, H. & Shaw, R. Observation of a self-limiting, shear-induced turbulent inversion layer above marine stratocumulus. *Bound.-layer. Meteorol.* **145**, 131–143 (2012).
12. Malinowski, S. P. et al. Physics of stratocumulus top (POST): turbulent mixing across capping inversion. *Atmos. Chem. Phys.* **13**, 12171–12186 (2013).
13. Yeom, J. M. et al. High-resolution measurements of microphysics and entrainment in marine stratocumulus clouds. *Q. J. R. Meteorological Soc.* **150**, 81–97 (2024).
14. Krueger, S. K., Su, C.-W. & McMurtry, P. A. Modeling entrainment and finescale mixing in cumulus clouds. *J. Atmos. Sci.* **54**, 2697–2712 (1997).
15. Lu, C., Liu, Y., Xu, X., Gao, S. & Sun, C. Entrainment, mixing, and their microphysical influences. *Fast Processes in Large-Scale Atmospheric Models: Progress, Challenges, and Opportunities* 87–120 (2023).
16. Burnet, F. & Brenguier, J.-L. Observational study of the entrainment-mixing process in warm convective clouds. *J. Atmos. Sci.* **64**, 1995–2011 (2007).
17. Lehmann, K., Siebert, H. & Shaw, R. A. Homogeneous and inhomogeneous mixing in cumulus clouds: Dependence on local turbulence structure. *J. Atmos. Sci.* **66**, 3641–3659 (2009).
18. Lu, C., Liu, Y. & Niu, S. Examination of turbulent entrainment-mixing mechanisms using a combined approach. *Journal of Geophysical Research: Atmospheres* **116** (2011).
19. Yeom, J. M., Yum, S. S., Liu, Y. & Lu, C. A study on the entrainment and mixing process in the continental stratocumulus clouds measured during the racoro campaign. *Atmos. Res.* **194**, 89–99 (2017).
20. Yeom, J. M. et al. Vertical variations of cloud microphysical relationships in marine stratocumulus clouds observed during the ace-ena campaign. *J. Geophys. Res.: Atmospheres* **126**, e2021JD034700 (2021).
21. Yeom, J. M. et al. Cloud microphysical response to entrainment and mixing is locally inhomogeneous and globally homogeneous: Evidence from the lab. *Proc. Natl Acad. Sci.* **120**, e2307354120 (2023).
22. Hill, A. A., Feingold, G. & Jiang, H. The influence of entrainment and mixing assumption on aerosol–cloud interactions in marine stratocumulus. *J. Atmos. Sci.* **66**, 1450–1464 (2009).
23. Wang, S., Wang, Q. & Feingold, G. Turbulence, condensation, and liquid water transport in numerically simulated nonprecipitating stratocumulus clouds. *J. Atmos. Sci.* **60**, 262–278 (2003).
24. Hoffmann, F., Glassmeier, F., Yamaguchi, T. & Feingold, G. Liquid water path steady states in stratocumulus: Insights from process-level emulation and mixed-layer theory. *J. Atmos. Sci.* **77**, 2203–2215 (2020).
25. Slawinska, J., Grabowski, W. W., Pawlowska, H. & Morrison, H. Droplet activation and mixing in large-eddy simulation of a shallow cumulus field. *J. Atmos. Sci.* **69**, 444–462 (2012).
26. Hoffmann, F., Raasch, S. & Noh, Y. Entrainment of aerosols and their activation in a shallow cumulus cloud studied with a coupled lcm–les approach. *Atmos. Res.* **156**, 43–57 (2015).
27. Yeom, J. M. et al. Impact of secondary droplet activation on the contrasting cloud microphysical relationships during the wet and dry seasons in the amazon. *Atmos. Res.* **230**, 104648 (2019).
28. Efraim, A. et al. Secondary droplet activation during condensational growth in convective clouds and its detection from satellites. *Atmos. Res.* **299**, 107196 (2024).
29. Hoffmann, F. & Feingold, G. Cloud microphysical implications for marine cloud brightening: the importance of the seeded particle size distribution. *J. Atmos. Sci.* **78**, 3247–3262 (2021).
30. Prabhakaran, P., Hoffmann, F. & Feingold, G. Evaluation of pulse aerosol forcing on marine stratocumulus clouds in the context of marine cloud brightening. *J. Atmos. Sci.* **80**, 1585–1604 (2023).
31. Sterzinger, L. J. & Igel, A. L. Above-cloud concentrations of cloud condensation nuclei help to sustain some arctic low-level clouds. *Atmos. Chem. Phys.* **24**, 3529–3540 (2024).
32. Wood, R. Stratocumulus clouds. *Monthly Weather Rev.* **140**, 2373–2423 (2012).
33. Chang, K. et al. A laboratory facility to study gas–aerosol–cloud interactions in a turbulent environment: The π chamber. *Bull. Am. Meteorol. Soc.* **97**, 2343–2358 (2016).
34. Wang, J. et al. Aerosol and cloud experiments in the eastern north atlantic (ace-ena). *Bull. Am. Meteorol. Soc.* **103**, E619–E641 (2022).
35. Chuang, P., Charlson, R. J. & Seinfeld, J. Kinetic limitations on droplet formation in clouds. *Nature* **390**, 594–596 (1997).
36. Yum, S. S. et al. Cloud microphysical relationships and their implication on entrainment and mixing mechanism for the stratocumulus clouds measured during the vocals project. *J. Geophys. Res.: Atmosph.* **120**, 5047–5069 (2015).
37. Krueger, S. K. Equilibrium droplet size distributions in a turbulent cloud chamber with uniform supersaturation. *Atmos. Chem. Phys.* **20**, 7895–7909 (2020).
38. Shaw, R. A. et al. Fast and slow microphysics regimes in a minimalist model of cloudy Rayleigh-Bénard convection. *Phys. Rev. Res.* **5**, 043018 (2023).
39. Liu, Y. & Daum, P. H. Indirect warming effect from dispersion forcing. *Nature* **419**, 580–581 (2002).

40. Liu, Y., Daum, P. H. & Yum, S. S. Analytical expression for the relative dispersion of the cloud droplet size distribution. *Geophysical research letters***33** (2006).
41. Martins, J. & Dias, M. S. The impact of smoke from forest fires on the spectral dispersion of cloud droplet size distributions in the amazonian region. *Environ. Res. Lett.* **4**, 015002 (2009).
42. Chandrakar, K. K., Cantrell, W., Kostinski, A. & Shaw, R. Dispersion aerosol indirect effect in turbulent clouds: laboratory measurements of effective radius. *Geophys. Res. Lett.* **45**, 10–738 (2018).
43. Anil Kumar, V. et al. Investigation of aerosol indirect effects on monsoon clouds using ground-based measurements over a high-altitude site in western ghats. *Atmos. Chem. Phys.* **16**, 8423–8430 (2016).
44. Wang, Y. et al. Diverse dispersion effects and parameterization of relative dispersion in urban fog in eastern china. *J. Geophys. Res.: Atmosph.* **128**, e2022JD037514 (2023).
45. Desai, N., Glienke, S., Fugal, J. & Shaw, R. Search for microphysical signatures of stochastic condensation in marine boundary layer clouds using airborne digital holography. *J. Geophys. Res.: Atmosph.* **124**, 2739–2752 (2019).
46. Nakajima, T., King, M. D., Spinhirne, J. D. & Radke, L. F. Determination of the optical thickness and effective particle radius of clouds from reflected solar radiation measurements. part ii: Marine stratocumulus observations. *J. Atmos. Sci.* **48**, 728–751 (1991).
47. Glenn, I. B., Feingold, G., Gristey, J. J. & Yamaguchi, T. Quantification of the radiative effect of aerosol–cloud interactions in shallow continental cumulus clouds. *J. Atmos. Sci.* **77**, 2905–2920 (2020).
48. Connolly, P., McFiggans, G., Wood, R. & Tsiamis, A. Factors determining the most efficient spray distribution for marine cloud brightening. *Philos. Trans. R. Soc. A: Math., Phys. Eng. Sci.* **372**, 20140056 (2014).
49. Considine, G. & Curry, J. A. Effects of entrainment and droplet sedimentation on the microphysical structure of stratus and stratocumulus clouds. *Q. J. R. Meteorol. Soc.* **124**, 123–150 (1998).
50. Schulz, B. & Mellado, J. P. Competing effects of droplet sedimentation and wind shear on entrainment in stratocumulus. *J. Adv. Modeling Earth Syst.* **11**, 1830–1846 (2019).
51. Chandrakar, K. K. et al. Aerosol indirect effect from turbulence-induced broadening of cloud-droplet size distributions. *Proc. Natl. Acad. Sci. USA* **113**, 14243–14248 (2016).
52. Khain, A., Rosenfeld, D. & Pokrovsky, A. Aerosol impact on the dynamics and microphysics of deep convective clouds. *Q. J. R. Meteorol. Soc.: A J. Atmos. Sci. Appl. Meteorol. Phys. Oceanogr.* **131**, 2639–2663 (2005).
53. Lee, S., Donner, L. & Penner, J. Thunderstorm and stratocumulus: how does their contrasting morphology affect their interactions with aerosols? *Atmos. Chem. Phys.* **10**, 6819–6837 (2010).
54. Storer, R. L., Van Den Heever, S. C. & Stephens, G. L. Modeling aerosol impacts on convective storms in different environments. *J. Atmos. Sci.* **67**, 3904–3915 (2010).
55. Grant, L. D. & van den Heever, S. C. Cold pool and precipitation responses to aerosol loading: modulation by dry layers. *J. Atmos. Sci.* **72**, 1398–1408 (2015).
56. Miltenberger, A. K. et al. Aerosol–cloud interactions in mixed-phase convective clouds–part 1: Aerosol perturbations. *Atmos. Chem. Phys.* **18**, 3119–3145 (2018).
57. Faloona, I. et al. Observations of entrainment in eastern pacific marine stratocumulus using three conserved scalars. *J. Atmos. Sci.* **62**, 3268–3285 (2005).

Acknowledgements

This work was supported by Department of Energy Office of Science grant number DE-SC0022128 and National Science Foundation grant number AGS-2113060. F.Y. was supported by the Office of Biological and Environmental Research in the Department of Energy, Office of Science, through the United States Department of Energy Contract No. DE-SC0012704 to Brookhaven National Laboratory.

Author contributions

J.M.Y., W.C., and R.A.S. designed the study. J.M.Y., H.F.S., J.C.A., W.C., and R.A.S. prepared the observations. J.M.Y., H.F.S., and J.C.A. conducted the observations. J.M.Y. analyzed the data. J.M.Y. and R.A.S. wrote the original paper. J.M.Y., H.F.S., J.C.A., F.Y., W.C., and R.A.S. reviewed the paper.

Competing interests

The authors declare no competing interests.

Additional information

Supplementary information The online version contains supplementary material available at https://doi.org/10.1038/s41612-024-00889-7.

Correspondence and requests for materials should be addressed to Jae Min Yeom, Will Cantrell or Raymond A. Shaw.